Influence of Static Seat Belt Fit Parameters on the Dynamic Response of the Large Omnidirectional Child Dummy in Frontal Impacts

Balaji Naga Sai Abhishikt Challa, Scott Noll, Colleen Bendig, Allison Louden

Abstract Proper seat belt fit is critical for child occupant protection, yet its influence on dynamic injury responses remains insufficiently characterised. This study investigated the effect of seat belt position relative to a 10-year-old occupant using the Large Omnidirectional Child (LODC) finite element (FE) model. Three belt fit metrics were defined: the shoulder belt wrap angle (α), the lap belt angle (β), and the shoulder belt score (SBS). The seat belt position was varied relative to the dummy's upright seating posture, and 101 simulations were conducted in LS-DYNA on the FMVSS No. 213b sled bench. Head acceleration, chest compression, abdominal pressures, belt forces, and head and knee excursions were independently screened for each seat belt metric using one-way analysis of variance (ANOVA) and Tukey–Kramer honestly significant difference (HSD) tests. All three metrics independently contributed to multiple injury outcomes. Head acceleration and chest compression were significantly influenced by SBS. Shoulder belt force was significantly influenced by β. Knee excursion was significantly influenced by both β and SBS. Abdominal pressures and forward excursions were influenced by all three factors. These findings identify the static belt fit metrics that individually affect the dynamic performance of the LODC FE model.

Keywords Child Safety, Finite Element, Large Omnidirectional Child, Occupant Kinematics, Seat Belt Fit

I. INTRODUCTION

Injury statistics from the Centers for Disease Control and Prevention (CDC) indicate that motor vehicle crashes (MVCs) are the leading cause of unintentional injury death in children aged 5 to 14 in the United States [1, 2]. The National Highway Traffic Safety Administration (NHTSA) reported that 161,478 children sustained injuries and 1,019 child fatalities occurred in vehicle crashes in 2023 [3]. Correct use of child restraint systems, including rear-facing child restraint systems (RFCRSs), forward-facing child restraint systems (FFCRSs), and belt-positioning boosters (BPBs), has been shown to minimise injuries in crashes [4–7]. Selection of the appropriate restraint system should be based on the child's age, height, and weight. Children under 12 years of age who are seated without boosters may adopt a slouched posture due to their shorter thigh lengths and seated heights, as they adjust to accommodate longer seat cushion lengths whilst keeping their lower legs parallel to the seat edge [8–10]. A slouched seating posture positions the shoulder belt across the neck and the lap belt directly over the abdomen, leading to a phenomenon known as submarining and a range of injuries collectively referred to as seat belt syndrome [8, 11–13]. The primary goal of a booster seat is to achieve optimal seat belt placement for children by positioning the shoulder belt across the midpoint of the clavicle and the lap belt below the anterior superior iliac spine (ASIS) on the anterior pelvis [14]. Distributing seat belt loads onto bony skeletal structures rather than soft tissues and organs has been shown to reduce the risk of injury in children during a crash [4, 15, 16].

Prior studies quantified seat belt position by defining the shoulder belt score (SBS) and lap belt score (LBS) using Hybrid III 6- and 10-year-old anthropomorphic test devices (ATDs) across boosters with distinct geometries and belt-routing features available in the United States [16–19]. These studies demonstrated that static belt fit scores varied substantially with booster design. Follow-up studies recruited child volunteers aged 5 to 12 years and seated them in different vehicle seat geometries and booster seat configurations to quantify static belt fit scores for each condition [20–21]. Comparisons between child volunteer belt fit scores and those obtained from similarly sized ATDs, including the Hybrid III 6- and 10-year-old, Q6, and Q10, revealed differences for the same boosters, highlighting anthropometric discrepancies and the limited postural biofidelity of the ATDs [21, 22]. Alongside these laboratory studies, naturalistic driving and observational studies demonstrated that children

Balaji Naga Sai Abhishikt Challa is a PhD student in Mechanical Engineering, and Scott Noll (noll.34@osu.edu) is a Research Assistant Professor in the Department of Mechanical and Aerospace Engineering, College of Engineering, Integrated Dynamics Laboratory, Simulation Innovation and Modeling Center, at The Ohio State University. Colleen Bendig is a Research Engineer at Transportation Research Center Inc., and Allison Louden is a Crashworthiness Research Engineer at the National Highway Traffic Safety Administration (NHTSA).

adopted different postures whilst seated in boosters depending on comfort level and external factors, such as the use of electronic or handheld devices [22–24]. These out-of-position (OOP) seating postures altered shoulder and lap belt scores and increased the likelihood of head contact with the vehicle interior [25].

Prior pre-crash manoeuvre studies further demonstrated that shoulder belt slip-off conditions altered belt fit by placing occupants in out-of-position postures [26–28]. These studies led to the establishment of additional quantification metrics, including maximum gap between the torso and shoulder belt, gap length, percentage of belt-to-torso contact, gap start location, and maximum gap location, used in conjunction with static belt fit scores [20]. Baker et al. [20] evaluated belt fit across various boosters incorporating these gap metrics and demonstrated the influence of booster geometry, lap belt anchorage position, and belt-routing features, particularly in the lap belt region. Designs that directed the lap belt away from the abdomen exhibited larger gaps between the torso and the shoulder belt. Commercially available boosters in the United States must pass dynamic frontal sled testing on a sled bench in compliance with Federal Motor Vehicle Safety Standard (FMVSS) No. 213b, as well as additional criteria [18]. The FMVSS No. 213/213b booster seat testing involves positioning an appropriately sized dummy in an upright seating posture on the booster, with the seat belt approximately crossing the mid-shoulder and the lap belt positioned below the ASIS [44]. However, prior research has shown that children adopt a range of seated postures [23–24, 29–30], and these postures affect seat belt fit in ways that are not accounted for in NHTSA's compliance testing.

Researchers have performed dynamic frontal sled tests using the Hybrid III 6- and 10-year-old ATDs and the Q10 ATD to examine the effects of varying belt fit and torso gap on injury response outcomes. Klinich et al. [17] conducted an extensive series of dynamic sled tests with the Hybrid III 10-year-old ATD to investigate the effects of booster design, lap belt geometry, and belt routing on kinematic and injury outcomes. They found that boosters with well-designed belt guides substantially reduced submarining and rollout, confirming that improvements in static belt fit directly enhance dynamic restraint performance. Reed et al. [19] further supported these findings by demonstrating that changes in booster seat design markedly affected lap and shoulder belt trajectories under dynamic loading, affirming that static belt geometry metrics are associated with ATD kinematic control during crash events. Klinich et al. [31] subsequently evaluated the Hybrid III 6- and 10-year-old ATDs dynamically on production vehicle seats and found that shorter seat cushions and steeper lap belt angles reduced head and knee excursions and mitigated submarining, confirming the relationship between static lap belt positioning and dynamic pelvic restraint. Baker et al. [8, 32] extended this understanding by introducing belt-to-torso contact measures and demonstrated through dynamic testing, which included the LODC, that insufficient initial belt contact amplified upper-torso excursion and rotation and reduced shoulder belt engagement in booster-seated ATDs. Collectively, these studies demonstrated that optimal belt positioning on the ATD produced favourable injury response outcomes, whereas deviations from the intended position resulted in adverse outcomes.

The Hybrid III 10-year-old ATD was developed by scaling down the Hybrid III 50th percentile male and is the largest ATD currently used to evaluate BPBs for older children under FMVSS No. 213b [33]. Research conducted using this ATD highlighted biofidelity concerns, particularly its rigid spinal structure, which caused chin-to-chest contact during sled testing and produced elevated head acceleration values [17, 32]. These biofidelity limitations were addressed by NHTSA through the development of the Large Omnidirectional Child (LODC) ATD. The LODC incorporates numerous modifications across its component subassemblies, resulting in an improved overall BioRank score of 1.21, compared to 2.70 for the Hybrid III 10-year-old [34–35]. BioRank score is a composite biofidelity rating that quantifies how closely an ATD's responses match reference post-mortem human subject data across a set of biomechanical tests, with lower scores indicating closer agreement [57]. A finite element (FE) model of the LODC was developed, with component-level qualification tests characterising the material properties of each subassembly against physical test responses [36, 38–41]. System-level sled test under FMVSS No. 213b conditions was subsequently used to validate the FE model, and strong correlation was obtained between the FE and physically measured responses [37].

Despite prior attempts to investigate the implications of initial belt fit on injury response, only a limited number of static belt fit configurations have been evaluated, and under a narrow range of test conditions. These configurations do not encompass the full set of static belt fit combinations that children encounter in real-world seating environments. Prior dynamic evaluations also revealed differing injury responses for comparable belt fit conditions across test configurations, indicating that additional factors influence the outcomes. The recently developed LODC ATD has been used to examine the effect of belt fit in only two studies [8, 32]. This gap presents an opportunity to further investigate the relationship between static belt fit and dynamic injury response in 10-year-old child occupants, contributing to improved occupant safety for older children. Given the complexities associated with experimental testing, injury biomechanics researchers frequently employ computational modelling as a complement to physical testing, enabling a broader range of parametric investigations [42]. The objective of this study was to examine the effect of belt fit on injury responses using the LODC FE model on the FMVSS No. 213b sled bench. A wide range of static belt fit configurations were simulated by maintaining the LODC in the upright seating posture, with the seat belt adjusted relative to the dummy. These configurations replicate the static belt fits reported in prior studies.

II. METHODS

Belt fit measurement parameters

The current study used three seat belt parameters to quantify seat belt position on the LODC ATD (Fig. 1). The shoulder belt wrap angle (α) was defined as the counterclockwise geometric angle measured between the normal projection of the seat back and the line to the D-ring from the side view (XZ-plane). The lap belt angle (β) was defined as the clockwise geometric angle measured between the normal projection of the seat base and the line to the inboard lap belt anchorage location from the side view providing a measure of the seat belt line of force acting upon the initial position of the ATD. A functional relationship exists between β and LBS that is dependent upon the seated posture of the ATD. Lower values of β position the lap belt segment directly over the abdomen, corresponding to a pre-submarined configuration. Higher values indicate that the lap belt lies flat on the thighs, away from the pelvis. The shoulder belt score (SBS) was calculated as the lateral distance between the ATD's mid-sagittal plane and the inboard edge of the shoulder belt segment, measured at the height of the upper ribcage stiffener [12, 14, 16–18]. A score of zero signifies that the inboard edge of the shoulder belt segment coincides with the mid-sagittal plane. A positive score indicates that the belt segment is located to the right of the mid-sagittal plane, whereas a negative score indicates that it is located to the left. A negative SBS indicates that the shoulder belt crosses over the neck, whilst an excessively positive SBS indicates that the shoulder belt segment is positioned far from the neck on the outer shoulder. Two representative sled test configurations are depicted in Fig. 2, showing the LODC FE model seated with the seat belts routed.

Simulation test matrix

Using the defined belt fit parameters, a simulation test matrix was generated to investigate the dynamic responses of the LODC across a wide range of belt positions relative to the occupant. The values of α and β were selected to span the full range of belt fit conditions reported in prior research, including both nominal belt placement and the extreme positions observed in children of varying stature, in slouched or out-of-position postures, and on boosters with differing belt-routing geometries [12, 15–22, 43]. Five levels were assigned to α (0°, 22.5°, 45°, 67.5°, and 90°) and β (0°, 22.5°, 45°, 67.5°, and 90°), and three levels to SBS (−40, 47, and 134 mm), yielding 75 simulation runs. A finer-resolution sweep was then conducted within $\alpha \in [35°, 60°]$ in increments of 6.25° and $\beta \in [25°, 45°]$ in increments of 5°, with SBS held constant at 0 mm, yielding an additional 25 runs. These narrower bounds corresponded to the static belt fit envelope consistently observed when children are properly seated on belt-positioning boosters. Across child volunteer studies involving more than 300 participants aged 4 to 12 and on the Hybrid III 6- and 10-year-old, Q6, Q10, and LODC ATDs, properly used boosters route the shoulder belt across the mid-shoulder and the lap belt below the ASIS, producing SBS and LBS values that cluster within a narrow band irrespective of upstream belt geometry [12, 15, 16, 19–22, 43]. Reed et al. [15] demonstrated that booster belt-routing features isolate the lap belt position at the pelvis from variations in the surrounding belt geometry, thereby constraining the at-body lap belt angle to this narrow band. The finer-resolution sweep was therefore targeted at the belt fit configurations most representative of properly boosted child occupants, whilst the wider sweep retained coverage of the extreme and out-of-position belt placements documented in naturalistic and observational studies [22–24, 26–28]. A baseline simulation was conducted with α = 53.05°, β = 27.5°, and SBS = −4 mm, representing the nominal seat belt configuration of the FMVSS No. 213b sled bench. In total, 101 simulations were run, and the simulation test matrix is presented in Fig. 3.

Simulation setup

The LODC FE model was seated on the FMVSS No. 213b sled bench in accordance with the FMVSS No. 213b standard [44]. The seat belts for each simulation run were routed across the ATD using Oasys PRIMER [45]. A combination of element types was used in modelling the seat belts across the ATD. Two-dimensional shell elements were employed for the primary shoulder and lap belt components that restrain the LODC ATD during the crash simulation. One-dimensional elements were used to connect the shoulder and lap belt components across three regions. First, these elements extended from the retractor to the shoulder belt segment through the inboard D-ring. Second, the shoulder and lap belt segments were connected at the inboard slip ring location. Third, one-dimensional elements extended from the lap belt segment to the outboard lap belt anchorage.

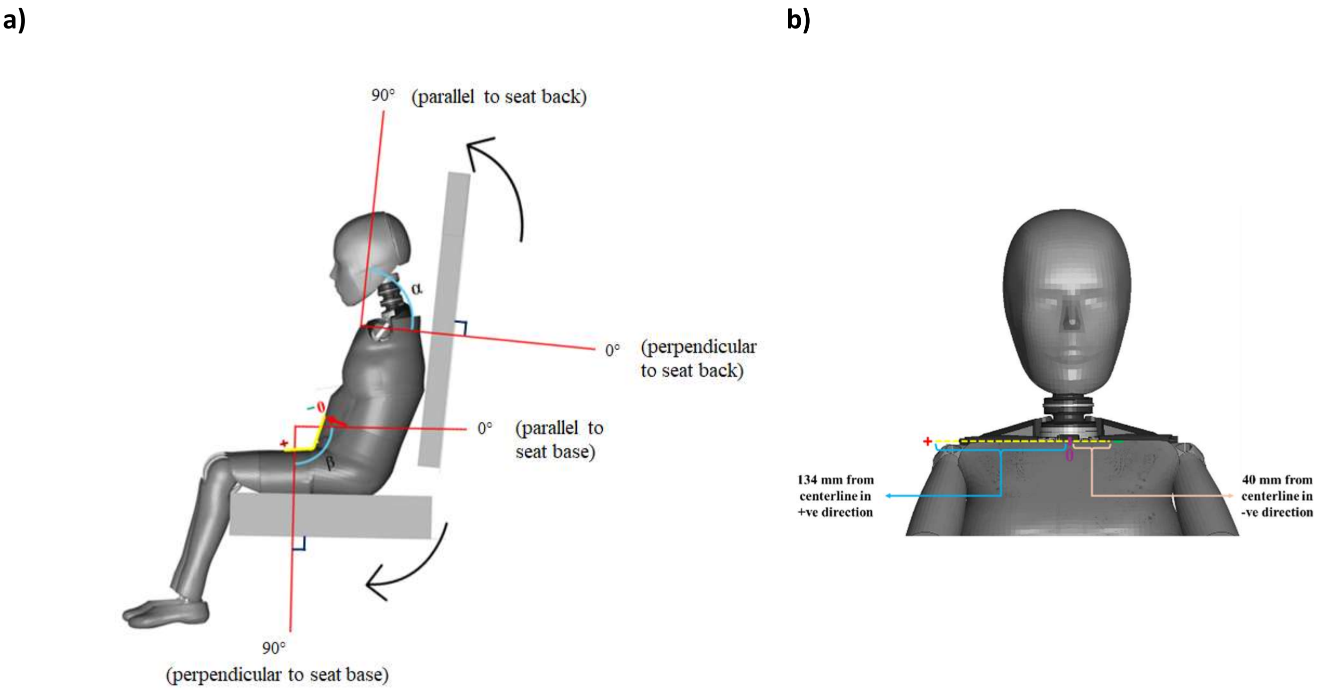

Fig. 1. (a) Side view (XZ-plane) illustrating the shoulder belt wrap angle (α), defined relative to the normal projection of the seat back, and the lap belt angle (β), defined relative to the normal projection of the seat pan. (b) Front view illustrating the shoulder belt score (SBS), defined as the lateral distance between the dummy's mid-sagittal plane and the inboard edge of the shoulder belt segment at the upper ribcage stiffener height.

An FMVSS No. 213b sled pulse with a peak deceleration of 21.9 g (delta-v = 13.1 m/s) at 9.92 ms was applied to the sled bench assembly using the BOUNDARY_PRESCRIBED_MOTION_RIGID keyword to simulate the frontal crash scenario [46]. A seat belt retractor was employed for the shoulder belt to achieve the standard pre-test belt tension of 13.3 N within the initial 3 ms, after which the retractor was deactivated to replicate the fixed belt condition equivalent to FMVSS No. 213b regulatory testing. For several combinations of α, β, and SBS, the belt segments were permitted to penetrate the seat back and base, to avoid the time-consuming modification of seat geometry for each case and to remove a confounding variable that could alter the belt routing path.

The static and dynamic coefficients of friction between the seat belt webbing and the LODC ATD surface were assumed as 0.7. This value lies at the upper end of the range reported in peer-reviewed FE crash simulation literature, which spans 0.1 to 0.6 for belt-to-occupant contact [47–48, 58]. Xiao et al. [47] demonstrated in a GHBMC frontal sled sensitivity sweep that higher coefficients permit non-trivial belt repositioning during the pre-loading phase. Brynskog et al. [48] identified belt friction as the dominant determinant of belt folding behaviour and belt-to-pelvis angle prior to restraint engagement. Selection of $\mu = 0.7$ represents an upper-bound intended to suppress belt slide during a simulation.

A termination time of 150 ms was set. The time step and mass scaling factor were 5×10^{-4} ms and 0.9, respectively. All 101 simulation runs were executed using the ls-dyna_smp_s_R14.0_515-g8a12796b62 solver [49] on a system equipped with 12 processors and 64 GB of RAM. Each run required approximately seven hours of CPU time to complete.

Data collection and analysis

Resultant head acceleration was derived from a node defined with the DATABASE_HISTORY_NODE_LOCAL keyword at the centre of gravity of the head, corresponding to the location of the head accelerometer in the physical LODC ATD. Chest compression was measured as the relative displacement in the x-direction between two nodes. The first node was located on the middle thoracic vertebral segment, and the second on the internal surface of the thoracic ribs at a normal projection from the vertebral segment, corresponding to the mid-thoracic chest deflection measurement location of the physical LODC. The LODC ATD incorporates twin abdomen pressure sensors (APTS) inserted in the abdominal slots to monitor the pressure exerted on the abdomen by seat belt loading. Abdomen pressures were recorded by enabling the rcforc output file via the DATABASE_ASCII_option keyword. A CONTACT_FORCE_TRANSDUCER_PENALTY contact definition was established between the fluid and cap components of the APTS. Shoulder and lap belt loads were recorded by enabling the sbtout output file via the DATABASE_ASCII_option keyword. Head and knee excursions were measured as displacement in the x-direction relative to a fixed node on the sled bench seat. Head excursion was tracked from the centre of gravity node of the head, and knee excursion from a node at the knee pivot location. Injury response outputs from the LODC ATD were extracted upon completion of each run and filtered in accordance with SAE J211 using channel filter classes (CFCs) ranging from CFC 60 to CFC 1000 [50].

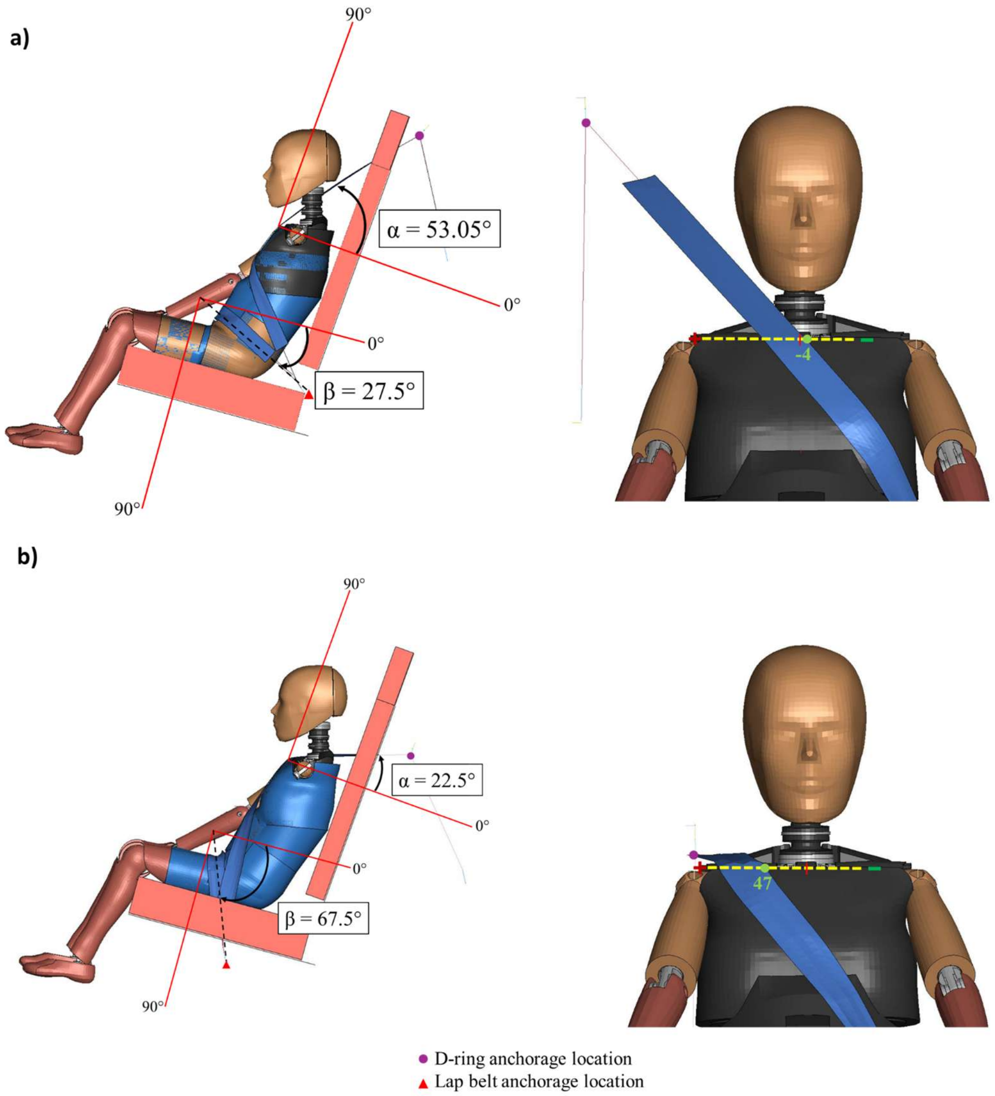

Fig. 2. Belt configurations for a) Run 101 (α = 53.05°, β = 27.5°, SBS = −4 mm) and b) Run 26 (α = 22.5°, β = 67.5°, SBS = 47 mm).

Following data extraction, JMP Pro 18 [51] was used to assess the influence of the defined static belt fit metrics on injury responses. Because each simulation was deterministic and yielded a single outcome per combination of α, β, and SBS, the analysis was structured as a screening study rather than a replicate-based statistical comparison. For each belt fit parameter (α, β, and SBS), the simulation runs were grouped by the discrete levels of that parameter, and the runs at each level were pooled across the other two parameters to form the observations within that group. A one-way analysis of variance (ANOVA) was conducted for the injury metrics with respect to each belt fit parameter, treating the fit parameter levels as categorical factors to determine the significance between groups using a post-hoc Tukey–Kramer HSD tests. A significance difference was assumed at *p < 0.05*. Each parameter was analysed independently and did not examine interaction effects between parameters.

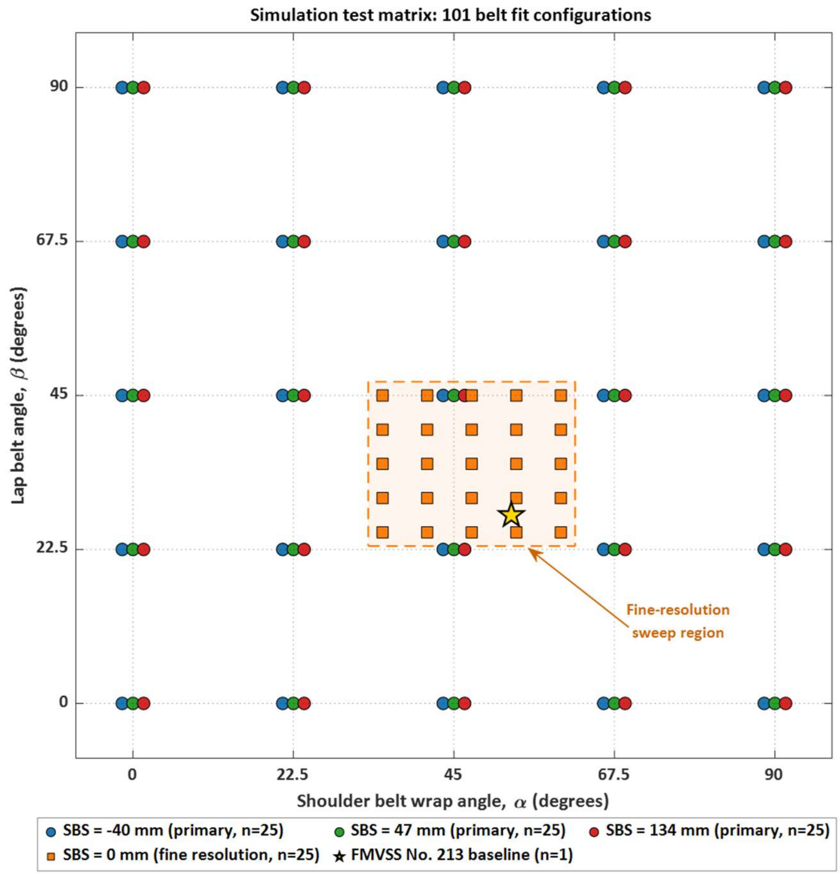

Fig. 3. Simulation test matrix showing all 101 belt fit configurations in the (α, β) plane. Circles denote the primary 75-run matrix, color-coded by shoulder belt score (SBS = −40, 47, and 134 mm); squares denote the additional 25 fine-resolution runs at SBS = 0 mm within the shaded region. The gold star indicates the baseline run at the FMVSS No. 213b sled bench configuration (α = 53.05°, β = 27.5°, SBS = −4 mm).

III. RESULTS

Run 74, with α = 90°, β = 90°, and SBS = 47 mm, was error-terminated at approximately 80 ms due to a negative volume error in the upper arm flesh component caused by excessive shoulder belt loading and was therefore excluded from the statistical analysis. Run 101, representing the FMVSS No. 213b sled bench belt configuration (α = 53.05°, β = 27.5°, SBS = −4 mm), was retained as a point of reference. An example of the dummy kinematics from Run 38 is shown in Fig. 4. Results from all the simulations are presented in the appendix Table AI.

Head Acceleration

One-way ANOVA showed that SBS significantly influenced peak head acceleration (p = 0.0179), whereas α (p = 0.0589) and β (p = 0.8982) was not significant (Table AII). Post hoc Tukey–Kramer HSD comparisons showed that, for SBS, the most inboard level (−40 mm: 112.06 ± 107.7 g) and the centred level (0 mm: 56.32 ± 1.7 g) formed distinct groups, whereas the 47 mm (63.22 ± 15.5 g) and 134 mm (88.3 ± 78.8 g) levels overlapped both. The means at the either extreme α, β, (0°, 67.5°, 90°) and SBS levels (-40 mm, 134 mm) were accompanied by large standard deviations. By contrast, the fine-resolution central configurations clustered tightly, near 55–58 g with standard deviations below 2 g (Fig. A1).

Chest Compression

By one-way ANOVA, SBS was the only significant factor that influenced chest compression ($p < 0.0001$), whereas neither α ($p = 0.8376$) nor β ($p = 0.9534$) produced significant effects (Table AIII). Post-hoc Tukey–Kramer HSD testing showed clear separation between the most inboard level, SBS = −40 mm (14.28 ± 5.1 mm), and the positive SBS levels (0 mm: 29.53 ± 1.3 mm, 47 mm: 33.11 ± 10.0 mm, 134 mm: 52.26 ± 8.4 mm). The most outboard level, SBS = 134 mm, produced the highest mean chest compression and formed a distinct group (Fig. A2).

Abdominal Pressures (RAPTS and LAPTS)

All three belt fit parameters significantly impacted both the right (RAPTS) and left (LAPTS) abdominal pressure responses ($p < 0.0001$; Tables AIV and AV). For RAPTS, the shallowest lap belt angle, β = 0° (16.22 ± 3.4 psi), and the steepest, β = 90° (14.23 ± 4.4 psi), produced elevated pressures relative to the intermediate β levels (22.5°, 25°, 30°, 35°, 40°, 45°, 67.5°). The same pattern was observed for α, with the shallowest, α = 0° (15.28 ± 2.5 psi), and the largest, α = 90° (15.92 ± 4.0 psi), produced higher pressures than the intermediate levels. For SBS, the most outboard level, SBS = 134 mm (15.34 ± 3.1 psi), and the most inboard level, SBS = −40 mm (12.11 ± 3.6 psi), were separated from the intermediate SBS levels (Fig. A3). LAPTS exhibited a similar pattern, with elevated pressures at β = 0° (13.09 ± 2.5 psi) and β = 90° (17.25 ± 4.8 psi), elevated pressures at α = 0° (15.68 ± 3.5 psi) and α = 90° (14.15 ± 4.8 psi), and clear separation between the negative and positive SBS levels. The most outboard level, SBS = 134 mm (17.82 ± 3.3 psi), produced the highest mean pressure (Fig. A4).

Seat belt Forces (Shoulder and Lap Belt)

For shoulder belt force, β was the only significant factor ($p < 0.0001$), whereas α ($p = 0.0919$) and SBS ($p = 0.6415$) were not significant (Table AVI). Post-hoc Tukey–Kramer HSD analysis showed that the steepest lap belt angles produced significantly larger shoulder belt forces, with β = 90° (9415.65 ± 1659.8 N) and β = 67.5° (7344.81 ± 1447.3 N) formed the two highest-force groups, distinct from one another and from the shallower β configurations, which overlapped (Fig. A5).

Lap belt force, in contrast, was significantly influenced by all three parameters (α: $p < 0.0001$; β: $p = 0.0003$; SBS: $p = 0.0029$) (Table AVII). The largest wrap angle, α = 90° (9379.25 ± 2544.2 N), and the steepest lap belt angle, β = 90° (8044.77 ± 2866.1 N), produced the largest lap belt forces, and the most inboard level, SBS = −40 mm (7269.74 ± 2327.9 N), yielded higher lap belt forces than the centred level, SBS = 0 mm (5416.41 ± 312.5 N) (Fig. A6).

Head Excursion

α ($p = 0.0017$), β ($p < 0.0001$), and SBS ($p < 0.0001$) all significantly influenced peak head excursion (Table AVIII). Post-hoc Tukey–Kramer HSD analysis showed that the largest excursions occurred at the extreme configurations, the largest wrap angle, α = 90° (383.97 ± 122.7 mm), and the steepest lap belt angle, β = 90° (434.65 ± 116.7 mm), each formed the highest-excursion group for its respective parameter. For SBS, the most outboard level, SBS = 134 mm (390.90 ± 104.1 mm), was clearly separated from the most inboard level, SBS = −40 mm (233.32 ± 91.6 mm), and the centred level, SBS = 0 mm (232.48 ± 11.5 mm) (Fig. A7).

Knee Excursion

β ($p < 0.0001$) and SBS ($p = 0.0017$) significantly influenced peak knee excursion, whereas α ($p = 0.1158$) was not significant (Table AIX). Post-hoc Tukey–Kramer HSD analysis showed that the steepest lap belt angles, β = 90° (290.07 ± 49.8 mm) and β = 67.5° (184.01 ± 18.9 mm), formed the two highest-excursion groups, whilst the remaining β levels overlapped. For SBS, the most inboard level, SBS = −40 mm (171.40 ± 89.9 mm), produced higher knee excursion than the centred level, SBS = 0 mm (93.87 ± 8.2 mm) (Fig. A8).

Side View **Top View** **Front View**

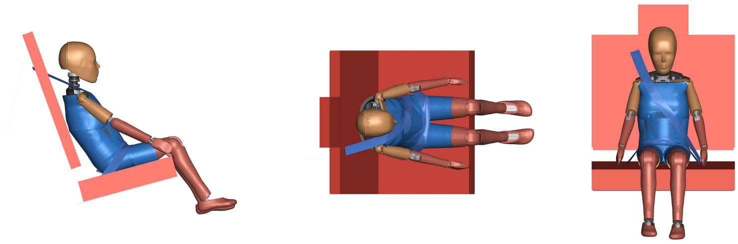

t = 0 ms

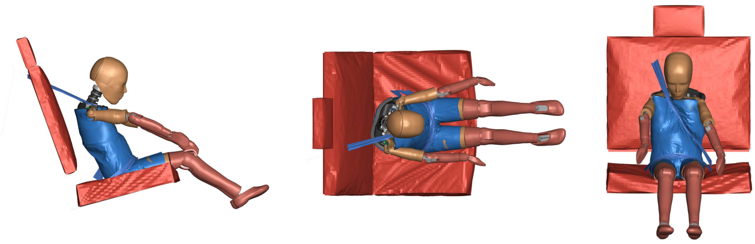

t = 50 ms

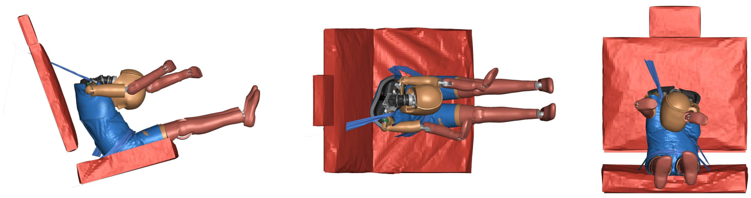

t = 90 ms

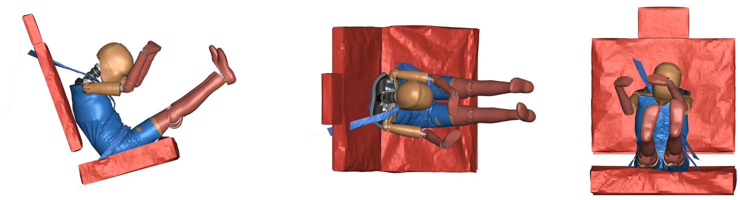

t = 120 ms

Fig. 4. LODC kinematics in side, top, and front view from run 38 for which α = 45°, β = 45°, and SBS = 47 mm.

IV. DISCUSSION

Head and abdominal injuries are the most common injuries sustained by children up to 12 years of age in vehicle accidents [53]. Head injuries typically occur in crashes involving contact between the head and the vehicle interior, or when the head experiences extreme accelerations or rotations [25]. Across the central range of belt fit configurations most representative of properly boosted child occupants, head acceleration was largely invariant to belt position, a pattern visible as the tightly grouped time histories in Fig. 5 (Column 1). This insensitivity is consistent with prior Hybrid III 10-year-old sled studies, which reported that vertical displacement of the D-ring did not alter head acceleration outcomes, including for boosters equipped with belt-routing guides [16]. At the extreme belt fit configurations, by contrast, several runs exhibited a sharp increase in head acceleration over a span of only a few milliseconds, evident in Fig. 5 (Column 1). These peaks resulted from secondary contact between the head and the upper arm during forward excursion. This brief, localised contact raised the peak head acceleration and produced the large standard deviations at the extreme levels. Peak head acceleration was therefore a comparatively insensitive and noisy discriminator of dynamic influence due to static belt fit for the LODC.

In contrast to head acceleration, head excursion was strongly sensitive to belt fit. At β = 90°, where the lap belt lies flat and far from the pelvis, mean head excursion was 384 mm, 52.3% higher than with the reference configuration. At SBS = 134 mm, where the shoulder belt sits off the shoulder on the upper arm, mean head excursion was 54% higher than with the reference configuration. Fig. 5 (Column 5) illustrates this: the head excursion time histories (solid lines) rise monotonically across each of the three parameter sweeps, with the peak magnitude increasing systematically as α, β, or SBS moves from its central to its extreme value. The knee excursion time histories (dashed lines), by contrast, are nearly constant across the α and SBS sweeps and rise sharply only at high β, consistent with the lap belt failing to restrain the pelvis when it is placed distally to the abdomen on the thighs rather than across the pelvic skeleton. These findings corroborate prior dynamic evaluations using the LODC and other ATDs, which reported elevated excursions when the belt was positioned far from the pelvis or laterally outboard on the clavicle [16, 17, 32]. Klinich et al. [31], evaluating Hybrid III 6- and 10-year-old ATDs on production vehicle seats, similarly reported that the worst kinematics occurred with the long cushion length and rearward lap belt geometry (the geometric analogue of high β), and that shortening the cushion and steepening the lap belt angle improved kinematic outcomes, particularly for the 10-year-old. Bohman et al. [25] previously identified head impact to the seat back as a leading cause of injury for belted, rear-seated children with abbreviated injury scale, AIS2+ head injuries. The head-excursion magnitudes observed at the extreme β and SBS configurations in the current study fall in the range that would enable such contact.

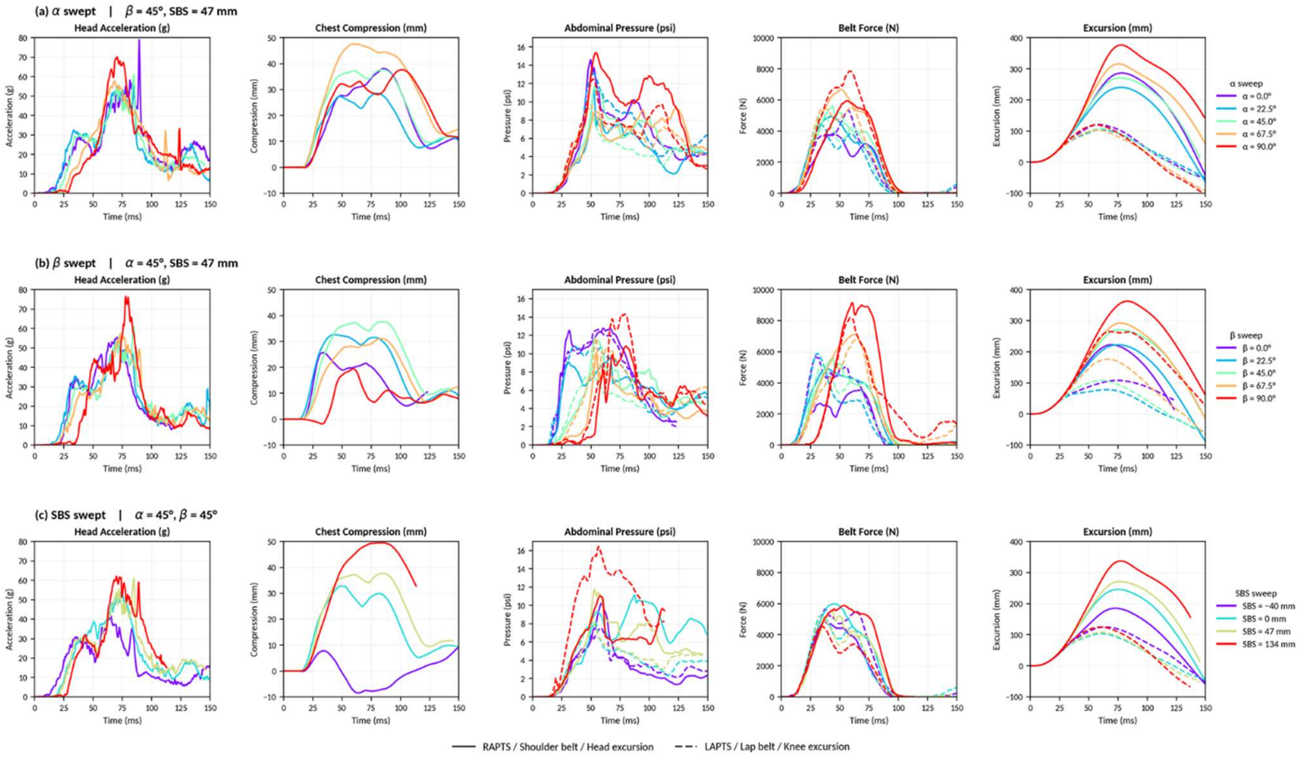

Fig. 5. Time-history sensitivity of LODC injury responses to single belt fit parameter variation. Each row sweeps one parameter while holding the other two constant: (a) α swept from 0° to 90° at β = 45°, SBS = 47 mm; (b) β swept from 0° to 90° at α = 45°, SBS = 47 mm; (c) SBS swept across −40, 0, 47, and 134 mm at α = 45°, β = 45°. Columns show, from left to right, head acceleration, chest compression, abdominal pressures (RAPTS solid, LAPTS dashed), belt forces (shoulder solid, lap dashed), and excursions (head solid, knee dashed).

Abdominal pressure exhibited clear differences in the time-history responses across belt fit configurations. The time histories in Fig. 5 (Column 3, Row b) reveal a consistent pattern in the timing and magnitude of the pressure rise as β varied. At the shallowest β configurations, the lap belt was placed directly over the abdomen anterior to the ASIS, in a pre-submarined position. The pressure responses therefore rose early in the event, shortly after the dummy initiated forward excursion. This early rise reflects direct loading of the abdomen by the lap belt, with the pelvis subsequently slipping beneath the belt and the occupant submarining [54]. The same mechanism is documented in children seated directly on the vehicle cushion without a booster, and in boosters where the lap belt routes higher than the ASIS [17, 31]. At intermediate β configurations, the pressure responses rose more gradually and to lower peak magnitudes, consistent with the lap belt transferring load primarily to the pelvic skeleton rather than to the soft abdominal tissue. At the extreme β = 90° configuration, where the lap belt laid distally to the abdomen on the thighs and provided minimal pelvic restraint at crash onset, the pressure responses showed no appreciable rise until approximately 50 ms, when the shoulder belt began loading the abdomen during maximum forward excursion.

Graci et al. [55] demonstrated the same mechanism with the LODC under moderate seat-back recline in 45° recline conditions without a booster, the lap belt moved upward off the ASIS into the abdominal pressure sensors, producing a mean peak pressure of 339.1 kPa compared with 73.7–168.4 kPa in the nominally seated conditions. The authors concluded that this pressure rise was direct evidence of submarining, with the pelvis rotating rearward and the belt loading the abdomen via the pressure sensors. The pressure response patterns observed across β in the current study mirror this transition, validating the APTS as a sensitive indicator of belt fit transitions between safe and submarining configurations.

Less expected was the finding that β = 90° configurations also produced abdominal pressures statistically indistinguishable from the β = 0° configurations, despite the lap belt not loading the abdomen directly. Inspection of five representative runs at the β = 90°, SBS = 134 mm condition (Runs 15, 30, 45, 60, and 75) at 90 ms revealed that the shoulder belt, rather than the lap belt, was loading the left abdomen during maximum forward excursion of the dummy (Fig. 6). This combination of a poorly positioned lap belt and an outboard shoulder belt redirected restraint loading onto the abdomen via the shoulder belt path, producing the elevated pressure responses. Although submarining is often quantified via ASIS load cell forces, only APTS data was examined for the scope of this investigation and thus no comparison information was available with Hybrid III 10-year-old ATD.

Chest compression showed the clearest monotonic dependence on SBS in the study. Fig. 5 (Column 2, Row c) shows the relationship directly: chest compression rises from approximately 10 mm at SBS = −40 mm to nearly 50 mm at SBS = 134 mm, a five-fold increase driven solely by the lateral position of the shoulder belt across the torso. The corresponding α and β sweeps in rows a and b show no equivalent monotonic dependence, with the chest compression responses remaining within a comparatively narrow band of approximately 25 to 40 mm across the full range of α and β. When SBS = −40 mm, the shoulder belt wrapped around the lower neck and travelled down toward the underarm with little engagement of the upper torso, producing the lowest chest compressions in the dataset. As SBS moved into the positive range of 0 to 47 mm, the belt spanned the torso evenly with high contact area, producing intermediate compressions consistent with proper restraint. At SBS = 134 mm, the shoulder belt was positioned beyond the clavicle, diagonally across the upper torso, and on the upper arm, loading the ribcage directly and producing the highest chest compression values observed in the study. Bohman and Fredriksson [56] confirmed that the Q10's two sternally located IR-TRACC sensors are positioned to detect compression along the canonical shoulder belt path. An off-shoulder shoulder belt routing displaces the load away from these sensors, a mechanism analogous to the low chest compression observed in the present study at SBS = −40 mm. Child volunteer studies have documented that children commonly adjust the shoulder belt away from the neck by pulling it to one side or placing it under the arm to feel more comfortable [5, 20]. O'Neil et al. [57] quantified this misuse in real-world booster-seated children and reported that under-arm and behind-back shoulder belt routing is a recurring observed pattern, not a hypothetical extreme. Certain boosters have also been observed to route the shoulder belt off the clavicle and across the upper arm [20].

The shoulder belt force was sensitive only to β, indicating that shoulder belt loading is governed by lower-torso restraint rather than by shoulder belt routing itself. Fig. 5 (Column 4) visualises this load-sharing mechanism. In the β sweep (Row b), both the shoulder belt force and the lap belt force rise monotonically with β, reaching a peak shoulder belt force of approximately 9000 N at β = 90°. In the α sweep (Row a) and the SBS sweep (Row c), the belt force responses overlap closely across the central range of each parameter, confirming that belt force redistribution is governed primarily by lap belt geometry rather than by shoulder belt routing or wrap angle. When β exceeded approximately 70°, the lap belt did not begin to restrain the lower extremities until maximum forward excursion, leaving the shoulder belt to carry the majority of the restraint load and producing abnormally high shoulder belt forces. When β was below approximately 30°, the lap belt engaged immediately as the dummy initiated forward excursion, reducing the shoulder belt force. At combined α and β configurations near 0°, the dummy slid down along the lap belt, lowering both belt forces. Klinich et al. observed the same load-sharing pattern in Hybrid III 10-year-old sled tests: shallower lap belt angles produced submarining, near-vertical lap belt angles produced rollout, and intermediate lap belt geometries produced the most balanced load distribution between the lap and shoulder belts [17, 31]. Baker et al. extended this finding to the LODC and Q10, reporting that larger initial belt-to-torso gap conditions produced lap and shoulder belt forces consistent with delayed lower-torso engagement [32, 33]. The lap belt force was sensitive to all three parameters, with most of the variation driven by the extreme α and β configurations. An SBS of −40 mm also yielded elevated lap belt forces because the lower shoulder belt position failed to restrain the upper torso, transferring more of the restraint demand to the lap belt. These force patterns reinforce the interpretation that proper lap belt engagement, which depends on a β configuration that places the lap belt across the pelvis at crash onset, is the primary determinant of balanced load sharing between the shoulder and lap belt segments.

Several limitations should be acknowledged. First, the present simulations used a static and dynamic friction coefficient between the seat belt webbing and the LODC surface without a friction sensitivity sweep. The extreme belt fit configurations evaluated here have not been independently corroborated through physical sled testing across the full range of belt fit conditions. Secondly, only the FMVSS No. 213b sled pulse was evaluated. The design space of crash severities, pulse shapes, and impact directions was not sampled, and no stochastic perturbation of input parameters was applied. Thirdly, no comparison was made to a paediatric human body model such as PIPER or THUMS paediatric, which would provide an independent check on the LODC FE response at the extreme belt fit configurations evaluated here. Future work will extend this simulation framework to cross-validate the LODC FE responses against a paediatric human body model and integrate load limiters and pretensioner effects.

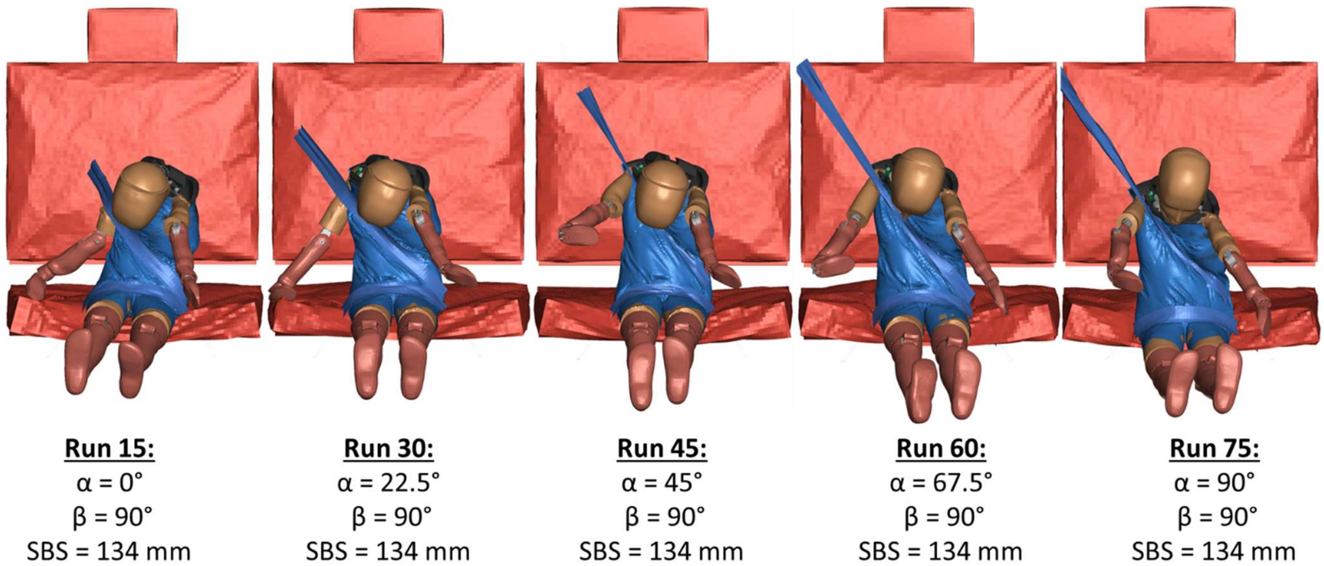

Fig. 6. LODC kinematics from front view at 90 ms from the runs 15, 30, 45, 60, and 75, all having β = 90° and SBS = 134 mm belt configurations with varying α levels.

V. CONCLUSION

The present study used the Large Omnidirectional Child (LODC) FE ATD to evaluate how static seat belt fit influences dummy response during frontal crashes. All three belt fit parameters, the shoulder belt wrap angle (α), the lap belt angle (β), and the shoulder belt score (SBS), contributed to one or more injury metrics. Head acceleration and chest compression were governed exclusively by SBS, shoulder belt force was governed exclusively by β, and knee excursion was governed by both β and SBS. The principal finding is that the LODC responses are insensitive to the central range of belt fit configurations and are sensitive at the extremes. Within the central region, representative of children who are properly seated on an appropriately used belt-positioning booster, variation in α, β, and SBS produced limited and largely non-significant differences in injury response. Adverse outcomes emerged exclusively when the belt was routed at extreme positions: the lap belt high on the abdomen or flat and far from the pelvis, and the shoulder belt against the neck or off the shoulder onto the upper arm. The screening framework therefore identifies a definite distinction between belt fit variations that matter and those that do not, with the boundary corresponding to documented belt fits.

VI. REFERENCES

[1] West, B. A., Rudd, R. A., Sauber-Schatz, E. K., Ballesteros, M. F. (2021) Unintentional injury deaths in children and youth, 2010–2019. Journal of Safety Research, 78: pp.322–330.

[2] Centers for Disease Control and Prevention (CDC). (2012) Vital signs: unintentional injury deaths among persons aged 0–19 years — United States, 2000–2009. MMWR Morbidity and Mortality Weekly Report, 61(15): pp.270–276.

[3] National Center for Statistics and Analysis. (2025) National Highway Traffic Safety Administration, Children: 2023 Data (Traffic Safety Facts, Report No. DOT HS 813 712), Washington, DC.

[4] Durbin, D., Elliott, M., Winston, F. (2003) Belt-positioning booster seats and reduction in risk of injury among children in vehicle crashes. Journal of the American Medical Association, 289(21): pp.2835–2840.

[5] Arbogast, K. B., Jermakian, J. S., Kallan, M. J., Durbin, D. R. (2009) Effectiveness of belt positioning booster seats: an updated assessment. Pediatrics, 124(5): pp.1281–1286.

[6] Arbogast, K. B., Kallan, M. J., Durbin, D. R. (2005) Effectiveness of high back and backless belt-positioning booster seats in side impact crashes. Annual Proceedings of the Association for the Advancement of Automotive Medicine, 49: pp.201–213.

[7] Eichelberger, A. H., Chouinard, A. O., Jermakian, J. S. (2012) Effects of booster seat laws on injury risk among children in crashes. Traffic Injury Prevention, 13(6): pp.631–639.

[8] Baker, G. H., Mansfield, J. A., Bolte, J. H., IV. (2024) Influence of initial belt torso contact on the kinematics and kinetics of booster-seated ATDs in frontal-oblique impacts. Traffic Injury Prevention, 25(sup1): pp.S183–S192.

[9] Huang, S., Reed, M. P. (2006) Comparison of child body dimensions with rear seat geometry. SAE Technical Paper 2006-01-1142.

[10] Bilston, L. E., Sagar, N. (2007) Geometry of rear seats and child restraints compared to child anthropometry. Stapp Car Crash Journal, 51: pp.275–298.

[11] Klinich, K. D., Ebert, S., Reed, M. P. (2016) University of Michigan Transportation Research Institute, Child Posture and Belt Fit in Second Row Vehicle Seats (UMTRI-2015-35), Ann Arbor, MI.

[12] West, B. A., Reed, M. P., Benedick, A., De Leonardis, D., Huey, R., Sauber-Schatz, E. (2022) Belt fit for children in vehicle seats with and without belt-positioning boosters. Traffic Injury Prevention, 23(8): pp.488–493.

[13] Parab, A., Whyte, T., et al. (2022) Can age or height define appropriate thresholds for transition to adult seat belts? An analysis of observed seat belt fit in children aged 7–12 years. International Journal of Environmental Research and Public Health, 19(3): p.1524.

[14] Chamouard, F., Tarriere, C., Baudrit, P. (1996) Protection of children on board vehicles: influence of pelvis design and thigh and abdomen stiffness on the submarining risk for dummies installed on a booster. Proceedings of the 15th International Technical Conference on Enhanced Safety of Vehicles, 1996, Washington, DC.

[15] Reed, M. P., Ebert-Hamilton, S. M., Klinich, K. D., Manary, M. A., Rupp, J. D. (2013) Effects of vehicle seat and belt geometry on belt fit for children with and without belt positioning booster seats. Accident Analysis & Prevention, 50: pp.512–522.

[16] Reed, M. P., Ebert-Hamilton, S. M., Klinich, K. D., Manary, M. A., Rupp, J. D. (2008) University of Michigan Transportation Research Institute, Assessing Child Belt Fit, Volume I: Effects of Vehicle Seat and Belt Geometry on Belt Fit for Children with and without Belt Positioning Booster Seats (UMTRI-2008-49-1), Ann Arbor, MI.

[17] Klinich, K. D., Reed, M. P., Ebert-Hamilton, S. M., Manary, M. A., Rupp, J. D. (2008) University of Michigan Transportation Research Institute, Assessing Child Belt Fit, Volume II: Effects of Restraint Configuration, Booster Seat Designs, Seating Procedure, and Belt Fit on the Dynamic Response of the Hybrid III 10-Year-Old ATD in Sled Tests (UMTRI-2008-49-2), Ann Arbor, MI.

[18] Reed, M. P., Ebert-Hamilton, S. M., Flannagan, C. A. C. (2013) National Highway Traffic Safety Administration, Improving the Repeatability and Reproducibility of Belt Fit Measurement with 6YO and 10YO ATDs (Report No. DOT HS 811 857), Washington, DC.

[19]Reed, M. P., Ebert, S. M., Sherwood, C. P., Klinich, K. D., Manary, M. A. (2009) Evaluation of the static belt fit provided by belt-positioning booster seats. Accident Analysis & Prevention, 41(3): pp.598–607.

[20]Baker, G. H., Mansfield, J. A., Hunter, R. L., Bolte, J. H., IV. (2021) Evaluation of static belt fit and belt torso contact for children on belt-positioning booster seats. Traffic Injury Prevention, 22(sup1): pp.S87–S92.

[21]Baker, G. H., Mansfield, J. A., Hunter, R. L., Bolte, J. H., IV. (2021) Comparison of child and ATD static belt fit and belt torso contact on belt-positioning booster seats. Proceedings of the International Research Council on the Biomechanics of Injury, 2021, pp.556–580.

[22]Baker, G. H., Bohman, K., Mansfield, J. A., Jakobsson, L., Bolte, J. H., IV. (2023) Comparison of child and ATD belt fit and posture on belt-positioning boosters during self-selected, holding device, and nominal conditions. Accident Analysis & Prevention, 192: p.107280.

[23]Arbogast, K. B., Kim, J., et al. (2016) Naturalistic driving study of rear seat child occupants: quantification of head position using a Kinect sensor. Traffic Injury Prevention, 17(sup1): pp.168–174.

[24]Osvalder, A. L., Hansson, I., Stockman, I., Carlsson, A., Bohman, K., Jakobsson, L. (2013) Older children's sitting postures, behaviour and comfort experience during ride — A comparison between an integrated booster cushion and a high-back booster. Proceedings of the 2013 IRCOBI Conference, 2013, Gothenburg, Sweden.

[25]Bohman, K., Arbogast, K. B., Bostrom, O. (2011) Head injury causation scenarios for belted, rear-seated children in frontal impacts. Traffic Injury Prevention, 12(1): pp.62–70.

[26]Bohman, K., Stockman, I., Jakobsson, L., Osvalder, A.-L., Bostrom, O., Arbogast, K. B. (2011) Kinematics and shoulder belt position of child rear seat passengers during vehicle maneuvers. Annals of Advances in Automotive Medicine, 55: pp.15–26.

[27]Baker, G. H., Stockman, I., et al. (2018) Kinematics and shoulder belt engagement of children on belt-positioning boosters during evasive steering maneuvers. Traffic Injury Prevention, 19(sup1): pp.S131–S138.

[28]Baker, G. H., Stockman, I., et al. (2017) Kinematics and shoulder belt engagement of children on belt-positioning boosters during emergency braking events. Proceedings of the International Research Council on the Biomechanics of Injury, 2017, Antwerp, Belgium, pp.327–340.

[29]Andersson, M., Bohman, K., Osvalder, A. L. (2010) Effect of booster seat design on children's choice of seating positions during naturalistic riding. Annals of Advances in Automotive Medicine, 54: p.171.

[30]Jakobsson, L., Bohman, K., Stockman, I., Andersson, M., Osvalder, A. L. (2011) Older children's sitting postures when riding in the rear seat. Proceedings of the IRCOBI Conference, 2011, pp.14–16.

[31]Klinich, K. D., Reed, M. P., Ebert, S. M., Rupp, J. D. (2014) Kinematics of pediatric crash dummies seated on vehicle seats with realistic belt geometry. Traffic Injury Prevention, 15(8): pp.866–874.

[32]Baker, G. H., Mansfield, J. A., Bolte, J. H., IV. (2022) Influence of initial belt torso contact on the kinematics and kinetics of booster-seated ATDs in frontal impacts. Proceedings of the International Research Council on the Biomechanics of Injury, 2022, Porto, pp.479–518.

[33]Mertz, H. J., Jarrett, K., Moss, S., Salloum, M., Zhao, Y. (2001) The Hybrid III 10-year-old dummy. Proceedings of the Stapp Car Crash Conference, 2001.

[34]Stammen, J., Moorhouse, K., Suntay, B., Carlson, M., Kang, Y. S. (2016) The large omnidirectional child (LODC) ATD: biofidelity comparison with the Hybrid III 10-year-old. Stapp Car Crash Journal, 60: p.581.

[35]Suntay, B., Stammen, J. A., Carlson, M., Ramachandra, R. (2021) Abdominal and thoracic injury risk functions for the large omni-directional child (LODC) ATD. Proceedings of the IRCOBI Conference, 2021, pp.537–555.

[36]Challa, A., Noll, S. (2025) The influence of impact location and angle on the dynamic response of a large omnidirectional child dummy head and neck complex. Proceedings of the WCX SAE World Congress Experience, 2025.

[37]Challa, B. N. S. A., Yang, P., Carlson, M., Suntay, B., Stammen, J., Noll, S. (2024) Development of a dynamic nonlinear finite element model of the large omnidirectional child crash test dummy. SAE International Journal of Advances and Current Practices in Mobility, 7(2024-01-2509): pp.430–447.

[38]Katangoori, D. R., Yang, P., et al. (2021) Development and calibration of the large omnidirectional child ATD head finite element model. SAE Technical Paper 2021-01-0922.

[39]Yang, P., Katangoori, D., et al. (2023) Development and validation of a dynamic abdominal pressure twin sensor finite element model. SAE International Journal of Transportation Safety, 11(3).

[40]Yang, P., Katangoori, D. R., Noll, S. (2023) Development and calibration of the large omnidirectional child ATD head and neck complex finite element model. SAE Technical Paper 2023-01-0557.

[41]Qualifications Procedures Manual, Large Omnidirectional Child, July 2022.

[42]Cereatti, A., Xu, T., et al. (2018) Development and validation of dummies and human models used in crash test. Applied Bionics and Biomechanics, 2018.

[43]Jones, M. L. H., Ebert, S., Manary, M. A., Reed, M. P., Klinich, K. D. (2020) Child posture and belt fit in a range of booster configurations. International Journal of Environmental Research and Public Health, 17(3): p.810.

[44]National Highway Traffic Safety Administration (NHTSA). (2015) Federal Motor Vehicle Safety Standard No. 213, Child Restraint Systems, pp.915–957.

[45]Oasys. "Oasys PRIMER User Manual (Version 21.1)", https://www.oasys-software.com/.

[46]National Highway Traffic Safety Administration (NHTSA). (2022) Federal Motor Vehicle Safety Standard No. 213a, Child Restraint Systems — Side Impact Protection, pp.39234–39317.

[47]Xiao, S., Yang, J., Forman, J., Panzer, M., Xiao, Z., Crandall, J. (2016) Effect of contact friction between seatbelt and human body model on simulation of rib fracture in frontal impact. Proceedings of the 2016 Eighth International Conference on Measuring Technology and Mechatronics Automation (ICMTMA), 2016, Macau, China, pp.255–257.

[48]Brynskog, E., Iraeus, J., et al. (2025) Simulating pelvis kinematics from belt and seat loading in frontal car crash scenarios: important boundary conditions that influence the outcome. Annals of Biomedical Engineering, 53: pp.441–470.

[49]Livermore Software Technology Corporation. (2001) LS-PrePost User's Manual, Livermore, CA.

[50]SAE International. (2018) Surface Vehicle Information Report: Sign Convention for Vehicle Crash Testing (SAE J1733).

[51]JMP Statistical Discovery LLC. (2024) Using JMP 18. JMP Statistical Discovery LLC, Cary, NC.

[52]O'Neil, J., Daniels, D. M., Talty, J. L., Bull, M. J. (2009) Seat belt misuse among children transported in belt-positioning booster seats. Accident Analysis & Prevention, 41(3): pp.425–429.

[53]Durbin, D. R., Chen, I., Smith, R., Elliott, M. R., Winston, F. K. (2005) Effects of seating position and appropriate restraint use on the risk of injury to children in motor vehicle crashes. Pediatrics, 115(3): pp.e305–e309.

[54]Lamielle, S., Vezin, P., et al. (2008) 3D deformation and dynamics of the human cadaver abdomen under seatbelt loading. Proceedings of the 52nd Stapp Car Crash Conference, 2008, San Antonio, Texas.

[55]Graci, V., Hauschild, H., Maheshwari, J., Humm, J. (2022) The effect of a moderately reclined seat-back angle on the kinematics of the Large-Omnidirectional Child Anthropomorphic Test Device with and without a belt-positioning booster in frontal crashes. Traffic Injury Prevention, 23(sup1): pp.S117–S122.

[56]Bohman, K., Fredriksson, R. (2014) Pretensioner loading to rear-seat occupants during static and dynamic testing. Traffic Injury Prevention, 15(sup1): pp.S111–S118.

[57]Wang, Z. J., Lee, E., et al. (2018) Biofidelity evaluation of THOR 5th percentile female ATD. Proceedings of the IRCOBI Conference, 2018.

[58]Poulard, D., Zhang, Q., Cochran, J. R., Gepner, B., Kerrigan, J. (2016) Quantitative evaluation of the occupant kinematic response of the THUMS 50th-percentile male model relative to PMHS laboratory rollover tests. Traffic Injury Prevention, 17(sup1): pp.101–108.

VII. APPENDIX

TABLE AI

LODC ATD kinetics and kinematics from all 101 frontal sled simulations

Run No.	Alpha	Beta	SBS	Peak Resultant Head Acceleration (g)	Peak Chest Compression (mm)	Peak APTS Right (psi)	Peak APTS Left (psi)	Peak Shoulder Belt Force (N)	Peak Lap Belt Force (N)	Peak Head Excursion (mm)	Peak Knee Excursion (mm)
1	0	0	-40	47.8	30	14.2	14.6	2530	5030	181	170
2	0	0	47	53.4	21	16.1	13.7	2427	4987	240	116
3	0	0	134	76.0	36	13.0	13.6	2386	6088	267	133
4	0	22.5	-40	57.7	8	16.6	12.6	2778	5074	212	112
5	0	22.5	47	60.2	28	15.7	16.6	3248	5312	259	91
6	0	22.5	134	112.00	42	14.9	18.9	3197	5265	301	81
7	0	45	-40	54.8	15	14.2	10.9	3575	4757	220	152
8	0	45	47	79.0	38	14.6	13.2	3851	5335	287	121
9	0	45	134	287.0	53	15.1	16.8	3872	4711	364	119
10	0	67.5	-40	60.8	16	14.2	14.3	5366	6915	222	228
11	0	67.5	47	125.0	27	14.9	18.3	5504	6318	295	189
12	0	67.5	134	215.0	46	16.0	22.0	6518	5536	378	160
13	0	90	-40	66.0	26	12.1	10.6	6957	5829	301	393
14	0	90	47	62.7	25	14.3	17.4	7252	5482	387	275
15	0	90	134	358.9	54	23.5	21.8	8874	4689	524	244
16	22.5	0	-40	50.2	16	12.2	8.9	3525	5753	147	114
17	22.5	0	47	48.5	24	12.8	10.3	2964	6045	207	68
18	22.5	0	134	44.8	46	15.4	12.1	3105	6780	272	61
19	22.5	22.5	-40	48.6	11	9.2	8.4	3863	5909	147	101
20	22.5	22.5	47	56.8	30	11.7	10.3	4090	5118	228	86
21	22.5	22.5	134	55.5	51	13.4	14.5	4248	5466	290	81
22	22.5	45	-40	48.8	10	13.6	9.1	4761	4889	153	117
23	22.5	45	47	55.4	29	11.3	10.4	4943	4487	240	104
24	22.5	45	134	48.2	53	14.5	17.6	5618	4274	333	101
25	22.5	67.5	-40	46.7	13	9.3	10.7	6068	5969	178	206
26	22.5	67.5	47	60.7	27	8.2	13.5	5522	4666	279	164
27	22.5	67.5	134	52.2	52	14.5	18.9	7452	5594	381	163
28	22.5	90	-40	60.7	13	11.8	13.7	7757	6274	266	274
29	22.5	90	47	73.0	19	14.9	18.8	8714	7225	350	270
30	22.5	90	134	53.3	51	21.2	22.6	10508	6287	498	255
31	45	0	-40	42.1	16	14.8	11.2	3933	6495	127	143
32	45	0	47	55.5	26	12.8	12.7	3528	5665	223	108
33	45	0	134	47.2	46	16.4	13.1	3311	5852	263	85
34	45	22.5	-40	163.2	12	8.6	7.2	4911	6537	138	90
35	45	22.5	47	54.3	33	9.5	10.8	4915	5884	223	78
36	45	22.5	134	54.8	52	11.6	15.7	4871	5591	300	74
37	45	45	-40	41.8	9	10.2	7.6	4873	5661	185	125
38	45	45	47	61.0	38	11.8	8.6	5620	5115	271	108
39	45	45	134	62.1	49	11.1	16.5	5882	4529	337	125
40	45	67.5	-40	37.2	11	6.9	5.8	6228	6438	193	184
41	45	67.5	47	57.4	31	10.1	11.7	7120	6842	292	176
42	45	67.5	134	56.7	49	9.7	17.7	8094	6086	370	161
43	45	90	-40	52.1	20	10.5	11.9	7851	7363	300	283

44	45	90	47	76.6	19	10.8	14.3	9154	8217	363	265
45	45	90	134	63.4	46	14.0	21.4	10201	7147	481	253
46	67.5	0	-40	262.1	10	16.1	12.0	4297	7728	154	78
47	67.5	0	47	46.0	34	16.7	11.5	3649	7270	254	63
48	67.5	0	134	47.8	53	17.0	14.0	3801	7249	306	64
49	67.5	22.5	-40	296.2	14	10.3	8.0	5209	7526	192	73
50	67.5	22.5	47	53.6	46	10.5	10.3	5608	6704	268	75
51	67.5	22.5	134	57.5	71	12.3	17.5	5051	6212	353	77
52	67.5	45	-40	270.6	12	8.7	7.4	5990	6415	225	101
53	67.5	45	47	57.7	48	9.3	9.6	6675	5550	316	103
54	67.5	45	134	60.6	54	13.7	17.8	6029	5157	401	100
55	67.5	67.5	-40	426.0	9	7.8	5.1	7529	9206	263	184
56	67.5	67.5	47	63.4	46	11.0	10.5	8490	8216	376	175
57	67.5	67.5	134	64.6	58	16.9	18.8	8492	8254	478	180
58	67.5	90	-40	43.2	12	6.1	9.2	9098	8799	360	267
59	67.5	90	47	61.7	46	11.9	18.4	11931	8169	504	258
60	67.5	90	134	64.6	54	14.3	21.8	12043	8930	567	280
61	90	0	-40	293.8	16	21.3	13.1	4682	8422	203	97
62	90	0	47	54.6	24	23.6	16.9	3870	7025	272	97
63	90	0	134	53.2	39	21.1	18.8	3706	7224	306	87
64	90	22.5	-40	62.4	18	16.0	8.6	6104	7883	259	80
65	90	22.5	47	59.9	55	12.1	12.9	5950	7213	323	79
66	90	22.5	134	61.1	72	14.0	17.7	5156	6811	392	79
67	90	45	-40	66.1	10	12.4	8.9	6001	10390	321	133
68	90	45	47	70.1	38	15.4	12.5	5944	7863	377	120
69	90	45	134	64.8	58	16.8	12.6	6087	7740	425	131
70	90	67.5	-40	101.8	16	9.2	6.1	9899	11673	350	202
71	90	67.5	47	70.7	45	11.3	11.0	9265	10852	429	193
72	90	67.5	134	67.0	62	15.8	19.4	8627	10000	535	196
73	90	90	-40	100.9	12	16.2	15.9	10299	14810	535	381
74	90	90	47		-	-	-	-	-	-	-
75	90	90	134	79.0	60	17.7	23.8	11180	13404	649	364
76	35	25	0	59.1	27	10.5	8.6	4618	5280	213	91
77	35	30	0	56.3	27	11.9	7.9	4819	5301	223	92
78	35	35	0	56.4	28	12.7	9.2	5183	5001	224	98
79	35	40	0	55.5	28	11.4	8.6	5489	4985	233	107
80	35	45	0	54.2	31	11.5	9.0	5561	4902	238	106
81	41.25	25	0	58.0	28	9.4	8.6	4815	5517	215	88
82	41.25	30	0	56.2	28	11.4	8.4	5090	5382	224	89
83	41.25	35	0	55.6	30	11.0	7.9	5361	5136	231	95
84	41.25	40	0	54.8	30	12.0	8.4	5740	5181	235	104
85	41.25	45	0	52.7	32	10.7	9.3	5784	5068	235	107
86	47.5	25	0	58.4	29	8.8	8.7	5174	5707	219	85
87	47.5	30	0	57.6	30	11.1	8.9	5447	5578	226	87
88	47.5	35	0	56.6	32	10.2	7.8	5707	5283	230	92
89	47.5	40	0	56.4	30	10.0	7.5	5698	5140	231	100
90	47.5	45	0	54.0	33	11.1	8.2	5980	5230	246	103
91	53.75	25	0	58.7	29	10.6	8.7	5394	5952	221	83
92	53.75	30	0	58.3	29	11.7	8.3	5667	5761	227	85

93	53.75	35	0	57.9	29	10.9	7.6	5844	5636	230	90
94	53.75	40	0	56.9	28	8.6	6.9	6129	5334	244	97
95	53.75	45	0	57.3	30	8.9	7.8	6125	5416	248	101
96	60	25	0	56.9	30	10.4	8.8	5605	6000	231	80
97	60	30	0	57.2	30	11.7	8.3	5717	5926	234	81
98	60	35	0	55.4	29	10.1	7.6	5967	5514	244	88
99	60	40	0	54.5	30	8.9	7.3	6426	5753	251	97
100	60	45	0	53.1	30	9.0	6.7	6547	5424	260	99
101	53.05	27.5	-4	56.7	24	11.3	8.0	4924	5957	225	90

TABLE AII

Summary of peak head acceleration (g) across varying alpha, beta, and SBS configurations. Values are presented as mean ± standard deviation, with associated p-value for each factor.

Head Acceleration (g)										
Alpha	**p-value** = 0.0589									
	0°	**22.5°**	**35°**	**41.25°**	**45°**	**47.5°**	**53.75°**	**60°**	**67.5°**	**90°**
	114.42 ± 95.7	53.56 ± 7.2	56.3 ± 1.8	55.46 ± 2.0	61.64 ± 29.7	56.6 ± 1.6	57.82 ± 0.7	55.42 ± 1.7	125.04 ± 123.1	86.1 ± 61.6
Beta	**p-value** = 0.8982									
	0°	**22.5°**	**25°**	**30°**	**35°**	**40°**	**45°**	**67.5°**	**90°**	
	81.53 ± 80.3	83.58 ± 66.0	58.22 ± 0.8	57.12 ± 0.9	55.38 ± 1.0	55.68 ± 1.0	79.96 ± 68.5	100.34 ± 100.2	86.86 ± 79.5	
SBS	**p-value** = 0.0179									
	-40 mm	**0 mm**	**47 mm**	**134 mm**						
	112.06 ± 107.7	56.32 ± 1.7	63.22 ± 15.5	88.3 ± 78.8						

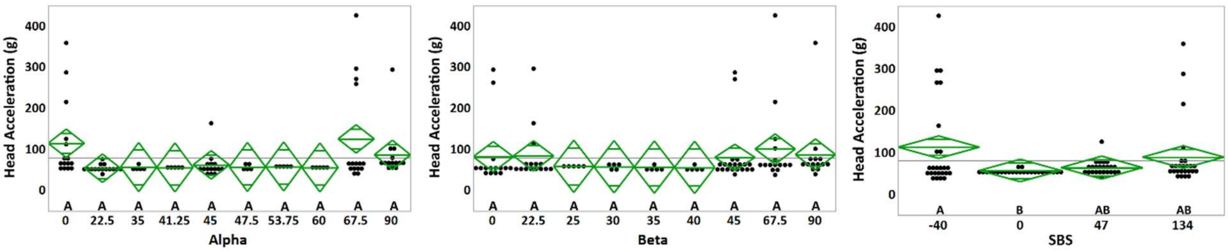

Fig. A1. Effect of alpha, beta, and SBS on peak head acceleration (g). Scatter points represent individual simulation results, and green diamonds denote group means with 95% confidence intervals. Connecting letters at each level indicate statistically similar and different groups based on Tukey–Kramer post hoc comparisons.

TABLE AIII

Summary of chest compression (mm) across varying alpha, beta, and SBS configurations. Values are presented as mean ± standard deviation, with associated p-value for each factor.

Chest Compression (mm)										
Alpha	**p-value** = 0.8376									
	0°	**22.5°**	**35°**	**41.25°**	**45°**	**47.5°**	**53.75°**	**60°**	**67.5°**	**90°**
	31.10 ± 13.6	29.61 ± 16.5	28.43 ± 1.4	29.46 ± 1.3	30.47 ± 15.4	30.82 ± 1.6	29.16 ± 0.6	29.79 ± 0.5	37.77 ± 20.9	37.41 ± 21.4
Beta	**p-value** = 0.9534									
	0°	**22.5°**	**25°**	**30°**	**35°**	**40°**	**45°**	**67.5°**	**90°**	
	29.12 ± 12.9	36.24 ± 21.3	28.71 ± 1.1	29.04 ± 1.1	29.64 ± 1.5	29.15 ± 0.7	33.50 ± 15.9	33.81 ± 18.1	32.58 ± 18.0	
SBS	**p-value** < 0.0001									
	-40 mm	**0 mm**	**47 mm**	**134 mm**						
	14.28 ± 5.1	29.53 ± 1.3	33.11 ± 10.0	52.26 ± 8.4						

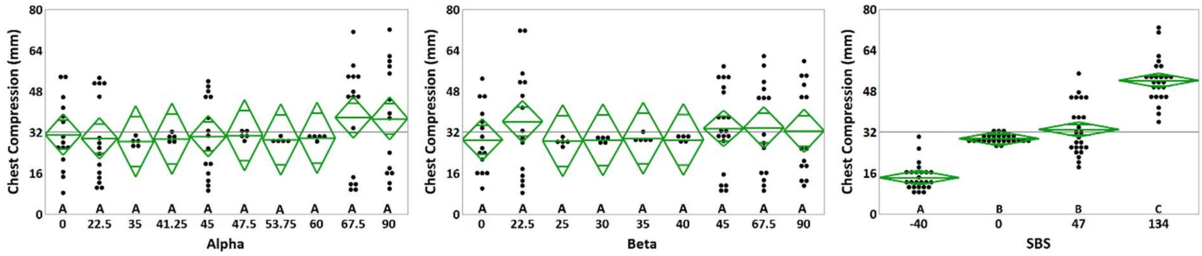

Fig. A2. Effect of alpha, beta, and SBS on chest compression (mm). Scatter points represent individual simulation results, and green diamonds denote group means with 95% confidence intervals. Connecting letters at each level indicate statistically similar and different groups based on Tukey–Kramer post hoc comparisons.

TABLE AIV

Summary of right abdomen pressure sensor (psi) across varying alpha, beta, and SBS configurations. Values are presented as mean ± standard deviation, with associated p-value for each factor.

Right Abdomen Pressure Sensor (RAPTS) (psi)										
Alpha	**p-value** < 0.0001									
	0°	**22.5°**	**35°**	**41.25°**	**45°**	**47.5°**	**53.75°**	**60°**	**67.5°**	**90°**
	15.28 ± 2.5	12.92 ± 3.1	11.60 ± 0.8	10.91 ± 1.0	11.25 ± 2.4	10.25 ± 0.9	10.16 ± 1.3	10.0 ± 1.1	12.17 ± 3.5	15.92 ± 4.0
Beta	**p-value** < 0.0001									
	0°	**22.5°**	**25°**	**30°**	**35°**		**40°**	**45°**	**67.5°**	**90°**
	16.22 ± 3.4	12.42 ± 2.6	9.96 ± 0.8	11.55 ± 0.3	10.97 ± 1.0		10.17 ± 1.5	12.20 ± 2.4	11.72 ± 3.3	14.23 ± 4.4
SBS	**p-value** < 0.0001									
	-40 mm			**0 mm**			**47 mm**			**134 mm**
	12.11 ± 3.6			10.58 ± 1.1			12.96 ± 3.2			15.34 ± 3.1

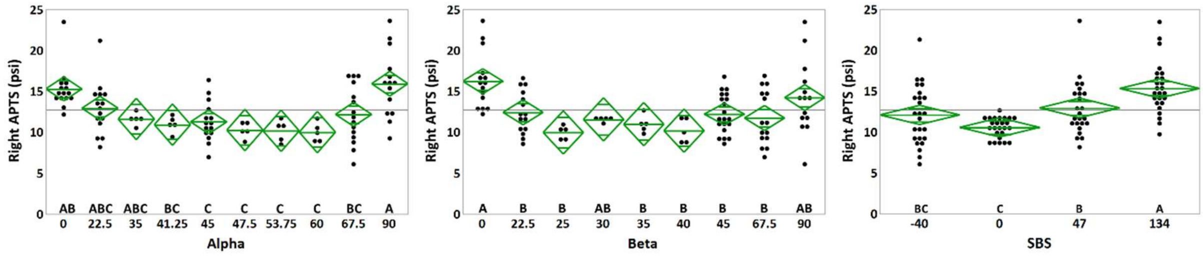

Fig. A3. Effect of alpha, beta, and SBS on right abdominal pressure sensor (psi). Scatter points represent individual simulation results, and green diamonds denote group means with 95% confidence intervals. Connecting letters at each level indicate statistically similar and different groups based on Tukey–Kramer post hoc comparisons.

TABLE AV

Summary of left abdomen pressure sensor (psi) across varying alpha, beta, and SBS configurations. Values are presented as mean ± standard deviation, with associated p-value for each factor.

Left Abdomen Pressure Sensor (LAPTS) (psi)										
Alpha	**p-value** < 0.0001									
	0°	**22.5°**	**35°**	**41.25°**	**45°**	**47.5°**	**53.75°**	**60°**	**67.5°**	**90°**
	15.68 ± 3.5	13.31 ± 4.3	8.65 ± 0.5	8.51 ± 0.5	12.40 ± 4.3	8.21 ± 0.5	7.87 ± 0.7	7.72 ± 0.8	12.79 ± 4.9	14.15 ± 4.8
Beta	**p-value** < 0.0001									
	0°	**22.5°**	**25°**	**30°**	**35°**		**40°**	**45°**	**67.5°**	**90°**
	13.09 ± 2.5	12.66 ± 3.9	8.68 ± 0.1	8.32 ± 0.3	8.02 ± 0.7		7.75 ± 0.7	11.02 ± 3.6	13.58 ± 5.5	17.25 ± 4.8
SBS	**p-value** < 0.0001									
	-40 mm			**0 mm**			**47 mm**			**134 mm**
	10.05 ± 2.9			8.19 ± 0.7			13.08 ± 3.0			17.82 ± 3.3

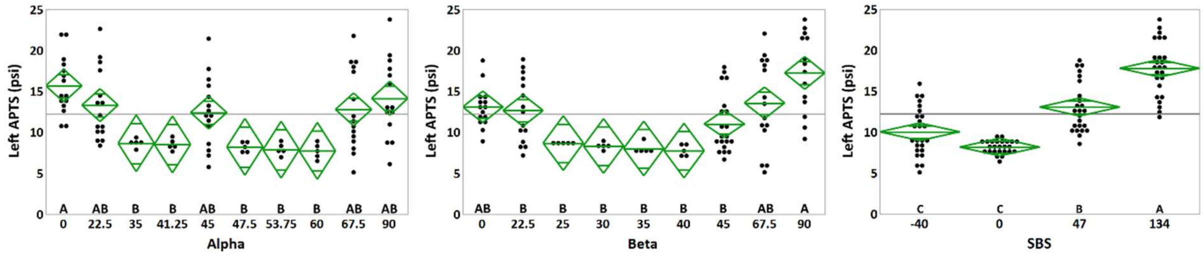

Fig. A4. Effect of alpha, beta, and SBS on left abdominal pressure sensor (psi). Scatter points represent individual simulation results, and green diamonds denote group means with 95% confidence intervals. Connecting letters at each level indicate statistically similar and different groups based on Tukey–Kramer post hoc comparisons.

TABLE AVI

Summary of shoulder belt force (N) across varying alpha, beta, and SBS configurations. Values are presented as mean ± standard deviation, with associated p-value for each factor.

Shoulder Belt Force (N)									
Alpha	**p-value** < 0.0919								
	0°	**22.5°**	**35°**	**41.25°**	**45°**	**47.5°**	**53.75°**	**60°**	**67.5°**	**90°**
	4555.58 ± 2054.3	5542.47 ± 2200.4	5133.80 ± 411.1	5358.14 ± 416.7	6032.83 ± 2059.5	5601.25 ± 305.2	5831.83 ± 313.6	6052.30 ± 419.8	6926.20 ± 2653.4	6911.93 ± 2460.4
Beta	**p-value** < 0.0001									
	0°	**22.5°**	**25°**	**30°**	**35°**	**40°**	**45°**	**67.5°**	**90°**	
	3447.49 ± 670.1	4613.28 ± 1010.5	5121.10 ± 405.6	5348.16 ± 385.7	5612.43 ± 330.1	5896.42 ± 375.7	5485.83 ± 880.1	7344.81 ± 1447.3	9415.65 ± 1659.8	
SBS	**p-value** < 0.6415									
	-40 mm	**0 mm**	**47 mm**	**134 mm**						
	5763.37 ± 2087.9	5595.46 ± 479.1	5842.98 ± 2369.3	6332.30 ± 2768.8						

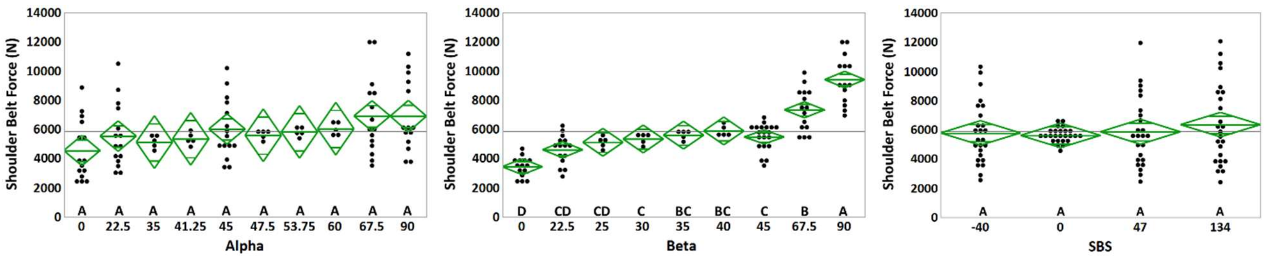

Fig. A5. Effect of alpha, beta, and SBS on shoulder belt force (N). Scatter points represent individual simulation results, and green diamonds denote group means with 95% confidence intervals. Connecting letters at each level indicate statistically similar and different groups based on Tukey–Kramer post hoc comparisons.

TABLE AVII

Summary of lap belt force (N) across varying alpha, beta, and SBS configurations. Values are presented as mean ± standard deviation, with associated p-value for each factor.

Lap Belt Force (N)										
Alpha	**p-value** < 0.0001									
	0°	**22.5°**	**35°**	**41.25°**	**45°**	**47.5°**	**53.75°**	**60°**	**67.5°**	**90°**
	5421.78 ± 635.3	5649.28 ± 845.1	5093.82 ± 183.6	5256.94 ± 186.3	6228.01 ± 930.9	5387.74 ± 242.5	5619.81 ± 251.8	5723.63 ± 250.9	7425.61 ± 1225.3	9379.25 ± 2544.2
Beta	**p-value** = 0.0003									
	0°	**22.5°**	**25°**	**30°**	**35°**	**40°**	**45°**	**67.5°**	**90°**	
	6507.44 ± 990.5	6166.96 ± 907.7	5691.18 ± 301.2	5589.77 ± 259.5	5314.11 ± 261.8	5278.77 ± 293.0	5645.69 ± 1467.1	7504.32 ± 2105.3	8044.77 ± 2866.1	
SBS	**p-value** < 0.0029									
	-40 mm	**0 mm**	**47 mm**	**134 mm**						
	7269.74 ± 2327.9	5416.41 ± 312.5	6481.72 ± 1490.3	6595.02 ± 1990.4						

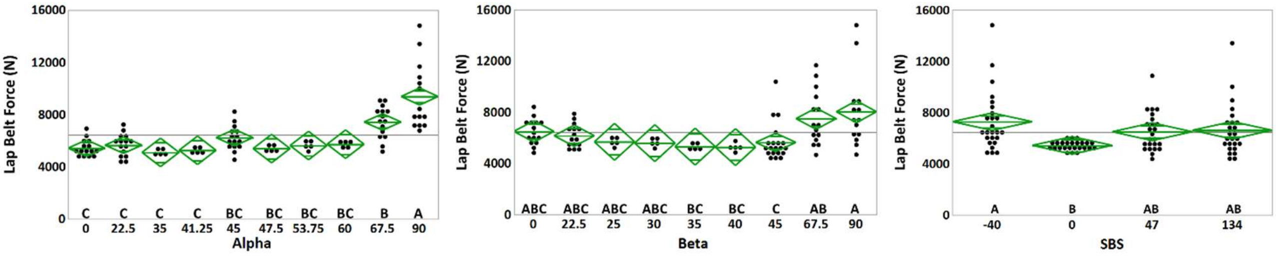

Fig. A6. Effect of alpha, beta, and SBS on lap belt force (N). Scatter points represent individual simulation results, and green diamonds denote group means with 95% confidence intervals. Connecting letters at each level indicate statistically similar and different groups based on Tukey–Kramer post hoc comparisons.

TABLE AVIII

Summary of peak head excursion (mm) across varying alpha, beta, and SBS configurations. Values are presented as mean ± standard deviation, with associated p-value for each factor.

Head Excursion (mm)										
Alpha	p-value = 0.0017									
	0°	22.5°	35°	41.25°	45°	47.5°	53.75°	60°	67.5°	90°
	295.81 ± 88.1	264.69 ± 97.6	226.17 ± 9.8	228.09 ± 8.8	271.08 ± 94.7	230.19 ± 9.9	233.89 ± 11.7	244.05 ± 11.7	334.48 ± 117.3	383.97 ± 122.7
Beta	p-value < 0.0001									
	0°	22.5°	25°	30°	35°	40°	45°	67.5°	90°	
	228.10 ± 56.9	259.01 ± 71.3	219.81 ± 7.2	226.64 ± 4.4	231.58 ± 7.5	238.93 ± 8.4	284.17 ± 72.8	334.58 ± 101.9	434.65 ± 116.7	
SBS	p-value < 0.0001									
	-40 mm	0 mm	47 mm	134 mm						
	233.32 ± 91.6	232.48 ± 11.5	302.55 ± 73.6	390.90 ± 104.1						

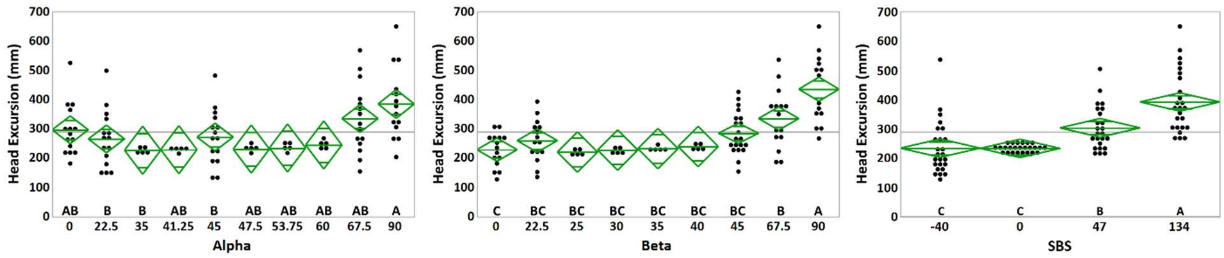

Fig. A7. Effect of alpha, beta, and SBS on peak head excursion (mm). Scatter points represent individual simulation results, and green diamonds denote group means with 95% confidence intervals Connecting letters at each level indicate statistically similar and different groups based on Tukey–Kramer post hoc comparisons.

TABLE AIX

Summary of peak knee excursion (mm) across varying alpha, beta, and SBS configurations. Values are presented as mean ± standard deviation, with associated p-value for each factor.

Knee Excursion (mm)										
Alpha	p-value = 0.1158									
	0°	22.5°	35°	41.25°	45°	47.5°	53.75°	60°	67.5°	90°
	172.25 ± 83.2	144.25 ± 74.0	98.84 ± 7.3	96.6 ± 8.6	150.51 ± 69.3	93.43 ± 7.8	91.27 ± 7.6	89.17 ± 8.7	138.50 ± 78.85	159.86 ± 100.1
Beta	p-value < 0.0001									
	0°	22.5°	25°	30°	35°	40°	45°	67.5°	90°	
	98.88 ± 32.2	83.89 ± 10.8	85.68 ± 4.3	86.85 ± 4.1	92.62 ± 3.9	101.03 ± 4.2	113.68 ± 14.3	184.01 ± 18.9	290.07 ± 49.8	
SBS	p-value = 0.0017									
	-40 mm	0 mm	47 mm	134 mm						
	171.40 ± 89.9	93.87 ± 8.2	140.88 ± 68.8	146.18 ± 79.8						

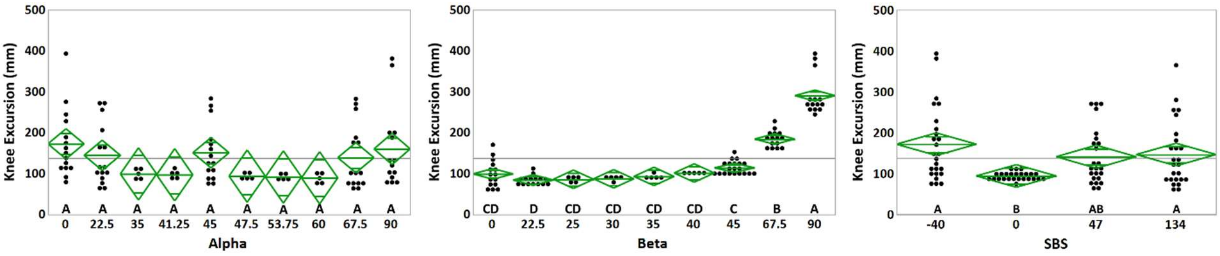

Fig. A8. Effect of alpha, beta, and SBS on peak knee excursion (mm). Scatter points represent individual simulation results, and green diamonds denote group means with 95% confidence intervals. Connecting letters at each level indicate statistically similar and different groups based on Tukey–Kramer post hoc comparisons.